OPEN

Resistive Memory for Harsh Electronics: Immunity to Surface Effect and High Corrosion Resistance *via* Surface Modification

Teng-Han Huang[1], Po-Kang Yang[1], Der-Hsien Lien[1], Chen-Fang Kang[1], Meng-Lin Tsai[1], Yu-Lun Chueh[2] & Jr-Hau He[1]

[1]Institute of Photonics and Optoelectronics & Department of Electrical Engineering, National Taiwan University, Taipei 10617, Taiwan, ROC, [2]Department of Materials Science and Engineering, National Tsing Hua University, Hsinchu 30013, Taiwan, ROC.

Correspondence and requests for materials should be addressed to J.-H.H. (jhhe@cc.ee. ntu.edu.tw)

The tolerance/resistance of the electronic devices to extremely harsh environments is of supreme interest. Surface effects and chemical corrosion adversely affect stability and operation uniformity of metal oxide resistive memories. To achieve the surrounding-independent behavior, the surface modification is introduced into the ZnO memristors *via* incorporating fluorine to replace the oxygen sites. F-Zn bonds is formed to prevent oxygen chemisorption and ZnO dissolution upon corrosive atmospheric exposure, which effectively improves switching characteristics against harmful surroundings. In addition, the fluorine doping stabilizes the cycling endurance and narrows the distribution of switching parameters. The outcomes provide valuable insights for future nonvolatile memory developments in harsh electronics.

ZnO has been widely investigated for potential applications in electronics and optoelectronics including transistors, photodetectors, gas sensors, strain sensors, dye-sensitized solar cells, and resistive random access memory (RRAM)[1–9]. Among these devices, gas sensors and photodetectors have achieved the outstanding sensitivity significantly benefited from the surface band bending due to the chemisorbed O_2 molecules, which is around 1.53 eV[10]. However, this surface effect is detrimental to some device applications, such as thin film transistors and RRAM because of surface effect-induced electrical instability[11,12].

The ZnO-based RRAM has attracted a great deal of attention due to its superior RRAM characteristics[13–15]. The resistive switching mechanism is associated with the formation/rupture of defects-based conductive nanofilaments near the interface between oxide and electrodes, which is enormously influenced by the chemisorbed O_2 molecules at the surfaces[5,12]. This leads to the fact that the resistive switching performances of oxide memory devices become sensitive to the ambiences, including switching yield and resistance value fluctuation[12]. Very recently Yang *et al.* reported that although the surface effect is a great calamity for RRAM, it can be suppressed by introducing graphene electrodes as a passivation layer *via* eliminating the detrimental effect of the chemisorbed O_2 molecules[5].

Harsh electronics as an emerging field is aiming to promote device capability and applicability in harsh environments. Related applications, including oil, gas, geothermal, aircraft/automotive engines, aerospace/military, and industrial uses, require devices to be operated in extremes of radiation, pressure, temperature, shock, and chemically corrosive liquids/gases environments[16,17]. For providing long-term reliability, sealed packaging is often applied to devices to deal with harsh conditions. Another way is to find/fabricate/modify the material as inert as possible in order to extend device lifetime. It has been reported that ZnO exhibits excellent irradiation resistance[18,19]. However, ZnO is extremely sensitive to corrosive atmospheric exposure and surface contamination associated with corrosion attack, limiting its practical use. For example, ZnO is chemically unstable in acetic conditions[20–22]. The formic acid molecules can weaken the Zn–O bonds, leading to Zn atom dissolution processes, which spreads throughout the material until the device failure occurs. Therefore, even though ZnO-based electronic and optoelectronic devices exhibit fascinating performances, severe surface effect and chemically instability would hinder ZnO-based electronic/optoelectronic device development. The ability for the devices to operate in various ambiences, including chemically harsh conditions, with long-term durability and reliability will play an important role in the successful emergence of resistive memory based on ZnO.

In this study, the surface/interface midification by CF_4 plasma treatment improves the resistive switching characteristics of the ZnO thin films. The statistical analysis including cycle-to-cycle and device-to-device tests over 120 cells shows that the fluorine incorporation into ZnO surfaces can effectively suppress the surface effect. This treatment not only prolongs the device endurance, but also stabilize the switching parameters, including set voltage (V_{set}), reset voltage (V_{reset}) and reset current. Moreover, the surface modification with fluorine allows the ZnO RRAM to withstand severe corrosive conditions. Improved RRAM characteristics, high inertness to surface effect, and high durability in acetic environment are due to surface passivation (saturating the dangling bonds and diminishing the oxygen vacancies) and strong Zn-F bonding (preventing the Zn atoms from dissolution) via the fluorine incorporation. To the best of our knowledge, no such beneficial functionalization has been reported for memory devices. It will be particularly useful to understand and develop surface modification for achieving desired device functions in extremely harsh applications.

Results

Fluorine dopants in the ZnO films. The chemical composition of the ZnO thin films with and without CF_4 plasma treatment was characterized by the X-ray photoelectron spectroscopy (XPS), as shown in Fig. 1 (a). Comparing to the pristine ZnO, the fluorinated ZnO thin films via CF_4 plasma treatment has a feature peak at 684.3 eV (F 1s peak), which is related to the F-Zn bond[23]. The F-Zn bond indicates the replacement of F for O after fluorination treatment, which changes the surface chemical composition of ZnO and thus is expected to modify the surface effect on the resistive switching behavior, which will be discussed later. Fig. 1 (b) shows the dependence of the CF_4 plasma treatment time on the fluorine content at the ZnO surface (characterized by XPS) and the resistance of ZnO thin films (measured at 0.1 V). As the fluorination time increases, the surface fluorine content increases. The ZnO thin film reaches a maximum fluorine content of 19.7 atomic% (at.%) at the ZnO surface after 10-min CF_4 plasma treatment. In the case of 20-min and 30-min plasma treatment, there is no further increase in the fluorine content.

One can see that the resistance decreases progressively with fluorination time. It has been reported that the fluorine in ZnO acts as effective dopants and surface passivation agents, decreasing the resistance due to the increase in carrier concentration and mobility and the elimination of surface effect[23,24]. Many surface defects including oxygen vacancies and dangling bonds can trap oxygen molecules to form chemisorbed $O_{2(ad)}^-$, which builds a high potential barrier on the surface[10,12,25]. Fluorine surface passivation for ZnO RRAM can remove the dangling bonds and diminish the oxygen vacancies by fluorine ions occupying at oxygen sites, preventing oxygen adsorption, eliminating the surface effect, and thus decreasing the resistance[23,24]. As shown in Fig. 1 (b), though the fluorine content was

saturated after >10 min fluorination treatment, the resistance was still decreased due to the thinning of ZnO thickness via the ion etching of CF_4 plasma (see Supplementary Fig. S1). As the fluorination time was increased from 0 to 30 min, the thickness was reduced from 100 nm to 85 nm, as shown in (see Supplementary Fig. S2). This leads to the fact that the surface also would become more damaged as the plasma treatment time is increased. The ZnO thin films with 10-min plasma treatments exhibit sufficient fluorine doping and is expected to suffer from less damage (as compared to the films with longer plasma treatment times). In contrast, the ZnO films with more-than-10-min plasma treatments greatly suffer from plasma-induced damages and thus deteriorate RRAM characteristics (not shown). Accordingly, the ZnO with 10-min plasma treatment is chosen to conduct the following RRAM characterizations and denoted as F-modified ZnO hereinafter. Note that the fluorine incorporation only occurs at the surface (within 10 nm), which has been characterized by the XPS depth profile (see Supplementary Fig. S3).

Resistive switching characteristics. Fig. 2 (a) shows I-V switching characteristics of pristine ZnO and F-modified ZnO devices. The forming process is necessary to initiate the switching behavior of the Pt/ZnO/Pt structure with a current compliance (I_{comp}). During the forming process, the initial resistance state is switched into the low resistance state (LRS). The forming voltage of the derived Pt/ZnO/Pt structure is approximate 3.5 V (see Supplementary Fig. S4). By applying small positive voltage without a I_{comp}, an abrupt drop of current occurs at the reset voltage (V_{reset}) and the LRS switches to the high resistance state (HRS). As sweeping to the positive bias again, the current increases suddenly at the set voltage (V_{set}); meanwhile, the resistance state is switched back to the LRS. In the set process, we applied the I_{comp} with 10 mA for both of pristine ZnO and F-modified ZnO to protect the devices from the permanent breakdown. Obviously, both of the ZnO devices show similar unipolar switching behavior, in which the larger positive bias induces the LRS and the smaller one sets the state to HRS. Though both of the ZnO thin films perform similar resistive switching behavior, the reset current for F-modified ZnO is lower than that for pristine ZnO, indicating the F-modified ZnO exhibits lower power consumption than pristine ZnO during memristive switching. The results are correspondent with the previous report that oxygen vacancies can be created by fluorine doping techniques in photocatalytic technology[26]. By introducing more dopants, more oxygen vacancies are generated, and low-powered operation switching conditions of RRAM devices can thus be expected[27].

In addition, the coexistence of bipolar and unipolar switching in resistive memory devices has been discussed extensively. The probabilities of switching yield of different operation modes are shown (see Supplementary Fig. S5). In comparison with the unipolar operation, the bipolar operation cannot reveal stable switching behaviors on both pristine (ZnO) and fluorinated device (F-modified ZnO). One can see that within the fixed number of devices which are chosen
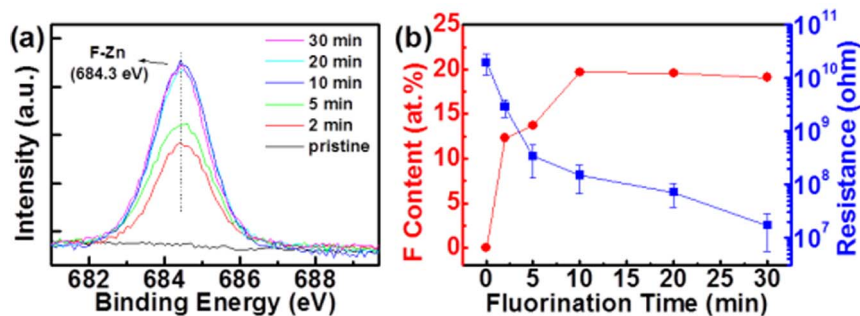

Figure 1 | (a) CF4 plasma treatment-dependent XPS spectra of F 1s for the ZnO films. (b) The dependence of the fluorination time on the F content at ZnO surfaces and the resistance of CF4 plasma-treated ZnO films.
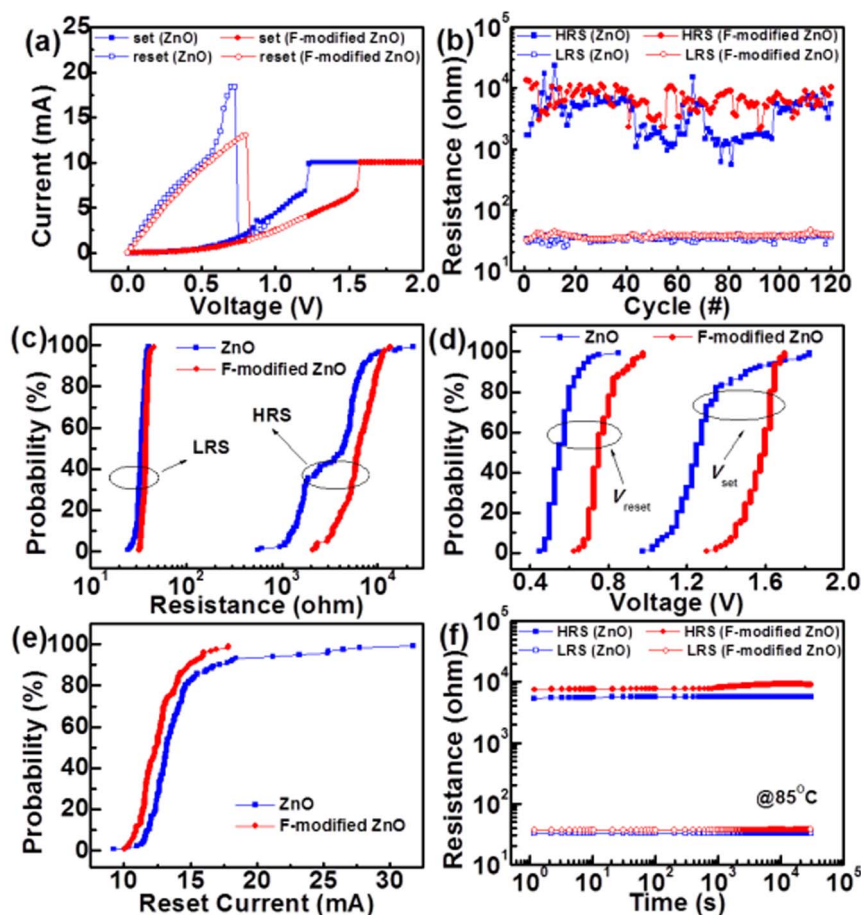
Figure 2 | (a) Typical unipolar resistive switching characteristics of the pristine ZnO and F-modified ZnO devices. (b) Endurance measurement of the pristine ZnO and F-modified ZnO devices for continuous 120 cycles at room temperature. The distributions of (c) HRS and LRS (d) V_{set} and V_{reset} (e) reset current of the pristine ZnO and F-modified ZnO devices. (f) Retention of the pristine ZnO and F-modified ZnO devices at 85°C.

randomly, unipolar switching is much more preferred because of comparatively high yield.

Fig. 2 (b) presents the endurance characteristics of pristine ZnO and F-modified ZnO devices. Note that the resistance of HRS and LRS was read out at 0.1 V. Clearly, during 120 switching cycles the HRS of the pristine ZnO device shows considerable fluctuation whereas the F-modified ZnO device performs more stable resistance values in the HRS. To illustrate the superior stability of the F-modified ZnO, we plotted the cumulative probability distribution of HRS and LRS, as shown in Fig. 2 (c). Both devices show concentrative distribution of LRS, while the cumulative probability of HRS between two devices exhibits a clear distinction. With the CF_4 plasma treatment, the coefficient of variation (COV, standard deviation divided by mean) of HRS of ZnO was greatly reduced from 77% to 38%, as shown in (Table 1). Consequently, in contrast to the wide dispersion of the HRS of the pristine ZnO devices, the F-modified ZnO ones sustain the memory window for almost 10^2. Moreover, the distributions of V_{set}, V_{reset}, and reset current of both devices are given in Figs. 2 (d)–(e). After the fluorination treatment, the COVs of V_{set}, V_{reset} and reset

current can be improved from 13% to 5%, 12% to 9%, and 24% to 12%, respectively (Table 1). Briefly, the excellent resistive switching uniformity is achieved by incorporating fluorine into ZnO, which is desperately required for practical resistive memory uses. Note that the better distribution of reset current prevents the device from extremely large current deviation, reducing the excessive power consumption during resistive switching[28]. The data retention test at 85°C is displayed in Fig. 2 (f). The HRS and the LRS in pristine ZnO and F-modified ZnO devices remain stable for 30000 sec. The F-modified ZnO device exhibits a larger memory window (i.e., HRS/LRS resistance ratio), indicating its splendid data retention capability. In short, the undesired switching parameter fluctuation is largely reduced due to the suppression of $O_{2(ad)}^-$ chemisorption at ZnO surfaces via fluorine passivation, indicating significant advantages of surface modification for use in the improvement of oxide RRAM characteristics. The relevant physical mechanism will be discussed later.

Oxygen chemisorption. It has been known that the $O_{2(ad)}^-$ chemisorption at metal oxide surfaces can play an important role

Table 1 | Statistics of switching parameters of the ZnO thin films. μ and COV are average value and coefficient of variation, respectively

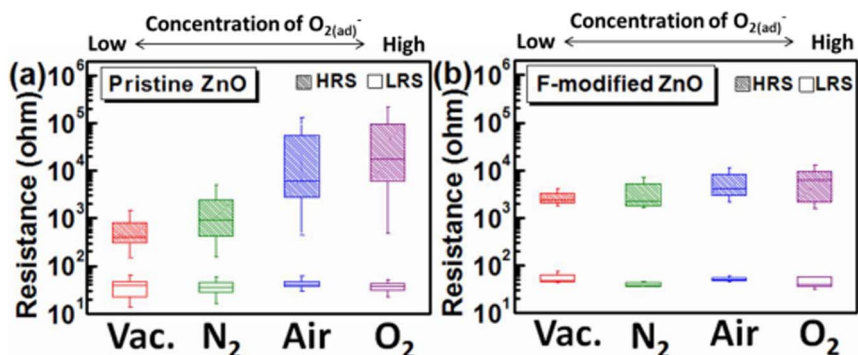| Sample	HRS (Ω)	LRS (Ω)	V_{set} (V)	V_{reset} (V)	I_{reset} (mA)
ZnO	μ = 4260.91 COV = 77%	μ = 33.68 COV = 9%	μ = 1.28 COV = 13%	μ = 0.56 COV = 12%	μ = 14.14 COV = 24%
F-modified ZnO	μ = 6736.97 COV = 38%	μ = 37.41 COV = 5%	μ = 1.56 COV = 5%	μ = 0.76 COV = 9%	μ = 12.66 COV = 12%

Figure 3 | Box and whisker plots for the atmosphere-dependent resistance in HRS and LRS of (a) pristine ZnO. (b) F-modified ZnO devices. The ambience of vacuum, nitrogen, air, and oxygen are denoted as Vac., N2, Air, and O2, respectively.

in tuning the electrical properties of metal oxide-based devices[5,10,12,29,30]. The O_2 molecules are adsorbed at the defective areas of metal oxide surfaces, serving as the traps for charge carriers to form chemisorbed $O_{2(ad)}^-$ and increase the surface potential. As a result, the conductivity of metal oxide surfaces is reduced, and this effect becomes even more pronounced as the oxygen partial pressure increases[10,25]. To investigate the importance of surface modification by fluorination, the resistance in HRS and LRS of pristine and F-modified ZnO devices were measured under different concentrations of $O_{2(ad)}^-$. Experiments were done by varying atmosphere conditions (vacuum, N_2, air, and O_2), as shown in Figs. 3 (a)–(b). In the four atmosphere conditions, the concentration of chemisorbed $O_{2(ad)}^-$ at ZnO surfaces at room temperature is vacuum $< N_2 <$ air $< O_2$. For pristine ZnO, as the oxygen partial pressure rises, more $O_{2(ad)}^-$ molecules are chemisorbed at the ZnO surface. Meanwhile, the HRS distributes in a higher and wider range, *i.e.*, increased mean values and fluctuation of HRS, as shown in Fig. 3 (a). By fluorinating the ZnO thin film, the undesired resistance fluctuation of the HRS is significantly reduced and the average HRS shows little dependence on the environmental atmosphere, as shown in Fig. 3 (b). This phenomenon could be ascribed to occurrence and elimination of surface effect caused by $O_{2(ad)}^-$ chemisorption and fluorine incorporation, respectively. For the pristine ZnO devices, the O_2 molecules adsorb at surface defects, such as oxygen vacancies and dangling bonds, and capture electrons to reduce the conductivity near the surface, resulting in the surface band bending effect. Consequently, the pronounced surface band bending effect increases the HRS resistance value of pristine ZnO memory, which would be aggravated by increasing $O_{2(ad)}^-$ concentration. After the fluorination of the ZnO thin film, the fluorine atoms could partially passivate the dangling bonds and replace the oxygen sites (forming the F-Zn bond). Hence, the surface effect on RRAM switching behaviors can be eliminated by suppressing the $O_{2(ad)}^-$ chemisorption *via* fluorine incorporation. As a result, HRS of the F-modified ZnO thin films becomes

insensitive to the ambience, revealing favorable advantage for practical applications in memory devices. While for the LRS, no apparent variation in LRS is observed under different oxygen partial pressures because the metallic conductive nanofilaments in ZnO thin films dominate the transport behavior, causing the immunity for LRS against the surface effect.

Acidic corrosion. The atmospheric corrosion due to Zn dissolution is an extremely significant issue that needs to be addressed for the application in harsh electronics[20,21,31]. Here chemical resistance of ZnO memory devices was examined with the acid vapor treatment. The resistance in HRS and LRS of pristine ZnO and F-modified ZnO devices were measured before and after the acid treatment, as shown in Figs. 4 (a)–(b). When exposed to the acid vapor (formic acid), the memory window of pristine ZnO shows gradual degradation with time, and all pristine ZnO devices would fail after 5-hour corrosion, as shown in Fig. 4 (a). The result can be attributed to the formic acid molecules that causes the dissociation of ZnO near the surface, which could gradually decrease the HRS resistance value with exposure time. By fluorinating ZnO, the corrosion could be notably suppressed and the HRS resistance value exhibits little dependence on the acid vapor exposure, as shown in Fig. 4 (b). The Zn dissolution from the surface can be restrained by doping fluorine into ZnO surfaces. Since the Zn-F bond is stronger than the Zn-O bond due to the higher electronegativity of fluorine atom[32], the unwanted atmospheric corrosion can be suppressed.

Distributions of operation voltages including V_{set}, V_{reset}, and forming voltage were also measured with acid vapor treatments (see supplementary Fig. S6 and Fig. S7). Accordingly, the operation voltages shown little dependence on the acid vapor treatment can be observed for the F-modified ZnO RRAM device in comparison with the pristine ZnO device. Moreover, the durability limit of the F-modified ZnO RRAM device under acid vapor treatment is evaluated (see supplementary Fig. S8), the F-modified ZnO RRAM device exhibits gradual degradation on memory window through 10-hour acid vapor treatment. As can be seen, in addition to the successful
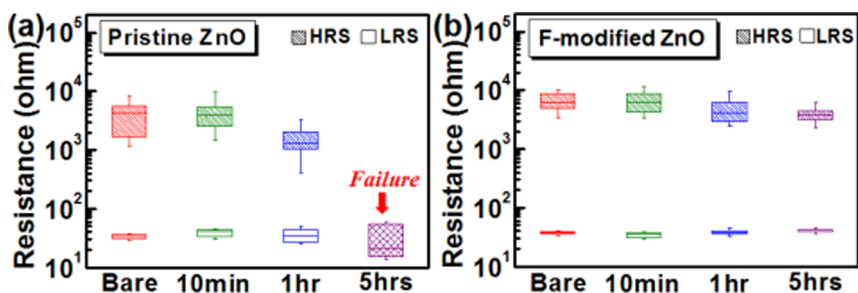

Figure 4 | Box and whisker plots for the resistance in HRS and LRS of (a) pristine ZnO. (b) F-modified ZnO devices with the acid vapor treatment.

elimination of surface effect, the F-modified ZnO memory performs excellent acid durability, indicating its admirable advantage for memristor applications in harsh electronics.

Discussion

In summary, the superior performance uniformity, and the high resistance to surface effect and corrosive environment of oxide memory devices are obtained *via* fluorine surface passivation (saturating the dangling bonds and diminishing the oxygen vacancies) and strong Zn-F bonding (preventing the Zn atoms from dissolution). High-performance oxide memory devices with immunity to surface effect and high chemical tolerance demonstrated here pave the way to harsh electronics.

Methods

Thin film growth and device characterization. 100-nm-thick ZnO thin films were deposited by sputtering on Pt/Ti/SiO$_2$/Si substrates with a pure ZnO (99.9% pure) target in an oxygen and argon mixture ambience at room temperature. The ratio of oxygen to argon ambient flow rate is 5 : 1. Subsequently, the ZnO film was put into plasma system to be fluorinated by the CF$_4$ plasma with 30 W. Electron-beam evaporation were used to deposit Pt top electrodes on ZnO-based thin films with 100 nm in thickness and 100 μm in diameter patterned by a metal shadow mask. The chemical composition of the ZnO films with and without CF$_4$ plasma treatment was investigated by XPS technique. The *I-V* characteristics were measured using a Keithley 4200 semiconductor parameter analyzer. During the measurement in voltage sweeping mode, the bias is defined as positive when the current flowed from top to bottom electrodes, and the negative bias is defined by the opposite direction. For box and whisker plots, the bottom and the top of the box are the 25th and the 75th percentile, the line near the middle of the box is the 50th percentile, and the ends of the whiskers represent the 10th percentile and the 90th percentile.

1. Yeh, L. K. *et al.* Giant Efficiency Enhancement of GaAs Solar Cells with Graded Antireflection Layers Based on Syringe like ZnO Nanorod Arrays. *Adv. Energy Mater.* **1**, 506–510 (2011).
2. Tsai, D. S. *et al.* Ultra-high-responsivity broadband detection of Si metal-semiconductor-metal Schottky photodetectors improved by ZnO nanorod arrays. *ACS Nano* **5**, 7748–7753 (2011).
3. Niu, S. *et al.* Enhanced Performance of Flexible ZnO Nanowire Based Room-Temperature Oxygen Sensors by Piezotronic Effect. *Adv. Mater.* **25**, 3701–3706 (2013).
4. Chen, M. W., Retamal, J. R. D., Chen, C. Y. & He, J. H. Photocarrier Relaxation Behavior of A Single ZnO Nanowire UV Photodetector: Effect of Surface Band Bending. *IEEE Electron Dev. Lett.* **33**, 411–413 (2012).
5. Yang, P. K. *et al.* Fully transparent resistive memory employing graphene electrodes for eliminating undesired surface effects. *Proc. IEEE* **101**, 1732–1739 (2013).
6. Chiang, Y. D. *et al.* Single-ZnO-Nanowire Memory. *IEEE Trans. Electron Dev.* **58**, 1735–1740 (2011).
7. Dong, Z. *et al.* Accurate Control of Multishelled ZnO Hollow Microspheres for Dye-Sensitized Solar Cells with High Efficiency. *Adv. Mater.* **24**, 1046–1049 (2012).
8. Lai, X., Halpert, J. E. & Wang, D. Recent advances in micro-/nano-structured hollow spheres for energy applications: From simple to complex systems. *Energy Environ. Sci.* **5**, 5604–5618 (2012).
9. Yi, L. *et al.* One dimensional CuInS$_2$–ZnS heterostructured nanomaterials as low-cost and high-performance counter electrodes of dye-sensitized solar cells. *Energy Environ. Sci.* **6**, 835–840 (2013).
10. Chen, C. Y. *et al.* Probing Surface Band Bending of Surface-Engineered Metal Oxide Nanowires. *ACS Nano* **6**, 9366–9372 (2012).
11. Kang, D. *et al.* Amorphous gallium indium zinc oxide thin film transistors: Sensitive to oxygen molecules. *Appl. Phys. Lett.* **90**, 192101 (2007).
12. Ke, J. J., Liu, Z. J., Kang, C. F., Lin, S. J. & He, J. H. Surface effect on resistive switching behaviors of ZnO. *Appl. Phys. Lett.* **99**, 192106 (2011).
13. Huang, T. H., Chang, W. Y., Chien, J. F., Kang, C. F., Yang, P. K., Chen, M. J. & He, J. H. Eliminating surface effects via employing nitrogen doping to significantly improve the stability and reliability of ZnO resistive memory. *J. Mater. Chem. C* **1**, 7593–7597 (2013).
14. Chang, W. Y., Lin, C. A., He, J. H. & Wu, T. B. Resistive switching behaviors of ZnO nanorod layers. *Appl. Phys. Lett.* **96**, 242109 (2010).
15. Huang, C. H. *et al.* ZnO$_{1-X}$ nanorod arrays/ZnO thin film bilayer structure: From homojunction diode and high performance resistive switching memory to a complementary 1D1R application. *ACS Nano* **6**, 8407–8414 (2012).
16. Tsai, D. S. *et al.* Solar-Blind Photodetectors for Harsh Electronics. *Sci. Rep.* **4**, 2628 (2013).
17. Tsai, D. S. *et al.* Trilayered MoS$_2$ Metal-Semiconductor-Metal Photodetectors: Photogain and Radiation Resistance. *IEEE J Sel Top Quant Electron.* **20**, 3800206 (2014).
18. Look, D. C., Reynolds, D. C., Hemsky, J. W., Jones, R. L. & Sizelove, J. R. Production and annealing of electron irradiation damage in ZnO. *Appl. Phys. Lett.* **75**, 811–813 (1999).
19. Coskun, C., Look, D. C., Farlow, G. C. & Sizelove, J. R. Radiation hardness of ZnO at low temperatures. *Semicond. Sci. Technol.* **19**, 752–754 (2004).
20. Zhou, J., Xu, N. & Wang, Z. L. Dissolving Behavior and Stability of ZnO Wires in Biofluids: A Study on Biodegradability and Biocompatibility of ZnO Nanostructures. *Adv. Mater.* **18**, 2432–2435 (2006).
21. Pern, F. J., Noufi, R., To, B., DeHart, C., Li, X. & Glick, S. H. Degradation of ZnO-based window layers for thin-film CIGS by accelerated stress exposures. *Proc. SPIE* **7048**, 70480P (2008).
22. Minami, T., Takata, S., Sato, H. & Sonohara, H. Properties of transparent zinc stannate conducting films prepared by radio frequency magnetron sputtering. *J. Vac. Sci. & Technol. A* **13**, 1095–1099 (1995).
23. Xu, H. Y. *et al.* F-doping effects on electrical and optical properties of ZnO nanocrystalline films. *Appl. Phys. Lett.* **86**, 123107 (2005).
24. Liu, B., Gu, M., Liu, X., Huang, S. & Ni, C. First-principles study of fluorine-doped zinc oxide. *Appl. Phys. Lett.* **97**, 122101 (2010).
25. Chen, C. Y. *et al.* Surface Effects on Optical and Electrical Properties of ZnO Nanostructures. *Pure Appl. Chem.* **82**, 2055–2073 (2010).
26. Li, D., Haneda, H., Labhsetwar, N., Hishita, S. & Ohashi, N. Visible-light-driven photocatalysis on fluorine-doped TiO$_2$ powders by the creation of surface oxygen vacancies. *Chem. Phys. Lett.* **401**, 579–584 (2005).
27. Tsunoda, K. *et al.* Low Power and High Speed Switching of Ti-doped NiO ReRAM under the Unipolar Voltage Source of less than 3 V. *IEDM Tech. Dig.* 767–770 (2007).
28. Hou, T. H. *et al.* Evolution of RESET current and filament morphology in low-power HfO$_2$ unipolar resistive switching memory. *Appl. Phys. Lett.* **98**, 103511 (2011).
29. Soci, C. *et al.* Nanowire Photodetectors. *J. Nanosci. Nanotechnol.* **10**, 1–20 (2010).
30. Ke, J. J., Tsai, K. T., Dai, Y. A. & He, J. H. Ultralow Contact Resistivity of Focused Ion Beam-Deposited Pt to Si Nanowire. *Appl. Phys. Lett.* **100**, 053503 (2012).
31. Hedberg, J., Baldelli, S. & Leygraf, C. Evidence for the Molecular Basis of Corrosion of Zinc Induced by Formic Acid using Sum Frequency Generation Spectroscopy. *J. Phys. Chem. Lett.* **1**, 1679–1682 (2010).
32. Tomat, E., Cuesta, L., Lynch, V. M. & Sessler, J. L. Binuclear fluoro-bridged zinc and cadmium complexes of a schiff base expanded porphyrin: fluoride abstraction from the tetrafluoroborate anion. *Inorg. Chem.* **46**, 6224–6226 (2007).

Author contributions

T.H.H., P.K.Y. and J.H.H. conceived and performed the experiment. T.H.H. and P.K.Y. wrote the main manuscript. D.H.L., P.K.Y., C.F.K., M.L.T. and Y.L.C. discussed the results and commented on the manuscript. J.H.H. supervised the project and finalized the manuscript.

Additional information